Journal of
Mechanical
Science and
Technology

Journal of Mechanical Science and Technology 21 (2007) 1129~1138

On the Near-field Aerodynamics of a Projectile Launched from a Ballistic Range

Rajesh Gopalapillai[a], Heuy-Dong Kim[a,*], Toshiaki Setoguchi[b], Shigeru Matsuo[b]

[a] *School of Mechanical Engineering, Andong National University, 388, Songchun-dong, Andong 760-749, Korea*
[b] *Department of Mechanical Engineering, Saga University, 1, Honjo-machi, Saga-shi, Saga 840-8502, Japan*

(Manuscript Received August 29, 2006; Received April 23, 2007; Accepted April 24, 2007)

Abstract

A computational fluid dynamics method has been applied to simulate the unsteady aerodynamics of the projectile launched from a ballistic range. A moving coordinate scheme for a multi-domain technique was employed to investigate the unsteady flow with moving boundary. The coordinate system fixed to each moving domain was applied to the multi-domains, and the effect of virtual mass was added in the governing equations for each domain. The unsteady, axisymmetric Euler equation systems were numerically solved using the third order Chakravarthy-Osher total variation diminishing scheme, with MUSCL approach. The projectile mass and configuration effects on the unsteady aerodynamics were investigated based on the computational results. The present computations were validated with results of some other CFD works available. The computed results reasonably capture the major flow features, such as shock waves, blast waves, shear layers, vertical flows, etc. which are generated in launching a projectile up to a supersonic speed. The present computational method properly predicts the velocity, acceleration and drag histories of the projectile.

Keywords: Moving coordinate method; Ballistic range; Unsteady drag; Shock wave; Supersonic flow

1. Introduction

The flow induced by a projectile launched from a ballistic range is very complicated, as it is associated with strong unsteadiness at the vicinity of the exit of the launch tube. When a projectile moves suddenly in the launch tube, a series of compression waves are formed ahead of it. These compression waves coalesce in a short distance of the tube, depending on the acceleration of the projectile and become a normal shock wave that propagates towards the exit of the launch tube. A blast wave is generated by the discharge of the shock wave from the exit of the launch tube, and shock wave diffraction occurs at the exit of the launch tube (Kim and Setoguchi, 1999; Kim et al., 2002), with an associated starting vortex. An unsteady jet is developed by the discharge of the gas in between the shock wave and the projectile. The projectile is then discharged from the launch tube, catches up and passes through the preceding unsteady jet and blast wave, and strong interactions among them cause unsteady loads acting on the projectile consequently influencing the flight stability of the projectile (Baker, 1974).

These complicated flow structures are typically observed in the near-field of the launch tube. Glass (1974) has shown detailed near-field structures using several visualization pictures of a bullet discharged from a rifle at initial Mach number 2. Schimdt & Shear (1975) have optically measured the muzzle blast waves and reported strong coupling between the

*Corresponding author. Tel.: +82 54 820 5622, Fax.: +82 54 823 5495
E-mail address: kimhd@andong.ac.kr

propellant gas flow and the blast wave. However, their visualization pictures were not clear enough to provide detailed near-field flow structures due to a dusty propellant gas. Erdos & Del Guidice (1975) have made some theoretical studies to investigate the blast wave and the propellant gas flow. Later, Merline & Dyment (1991) have tried to model the blast wave flow using a similarity law, based upon visualization pictures.

From these studies, the near-field flow structures of the launch tube are comparatively well known, but the near-field aerodynamics is hardly understood, because almost all of the related data are based on the qualitative optical visualizations. It is extremely difficult to experimentally investigate the projectile aerodynamics. Theoretical approach is also not easy due to the unsteadiness and three-dimensionalities, with strong compressibility effects involved in the projectile aerodynamics. More systematic study is needed to get the quantitative data with regard to the near-field projectile aerodynamics.

Another interesting flow phenomenon is obtained after the projectile passes through the blast wave, being quite different from the near-field mentioned above. The projectile flies at a supersonic speed, consequently leading to a shock wave system ahead of it. Under such a situation, the aerodynamics on the projectile may be associated with Mach number and Reynolds number, like the one which is obtained from a conventional supersonic wind tunnel test. However Mach number and Reynolds number become strongly dependant on time, because the projectile is considerably decelerated due to aerodynamic drag. In such a case, the projectile aerodynamics may be different from the steady aerodynamics, in which, at high-Reynolds number, the aerodynamics drag is only a function of only Mach number if the projectile shape were given (Pope and Goin, 1963; Sun et al., 2005). Moreover, the projectile mass can be one of the most important parameters in determining the unsteady aerodynamics, since it is directly related to the acceleration and deceleration of the projectile.

With the recent development in the computing capabilities and numerical schemes as well, computational fluid dynamics (CFD) is being recognized as the most effective research tool to investigate highly complicated flow phenomena. Jiang et al. (1998), have tried to numerically solve the blast flow fields using unsteady, axisymmetric, Euler equations which were discretized by the dispersion-controlled scheme, with moving boundary conditions. In their numerical simulations, a pre-cursor shock wave was assumed at the exit of a shock tube. After the discharge of the precursor shock, a projectile was also assumed to move at the same velocity as the post-shock velocity.

They have observed two blast waves at the vicinity of the tube exit, and they have argued that the release time between the precursor shock wave and the projectile has a negligible effect on the flow structures except in the region just behind the projectile. However, they have failed in showing the clear contact discontinuities which are, respectively, made from the discharge of the compressed gas ahead of the moving projectile inside the tube and the high-pressure propellant gas that is used to drive the projectile.

Recently, Takakura et al. [1997(a); 1997(b)], have used the moving coordinate method to simulate the unsteady projectile aerodynamics. They have testified the validity of their results using some experimental data. However, they assumed the initial velocity of the projectile while which should have been determined by computation. Thus their work is somewhat different from the aerodynamics of a real projectile which starts to move from a rest state inside the launch tube. They neither investigated the effects of the projectile mass and shape on the unsteady aerodynamics, nor provided the detailed aerodynamic data with regard to the projectile motions.

The present study is concerned with the near-field, unsteady aerodynamics of a projectile which is launched from a ballistic range. A computational fluid dynamic method has been applied to simulate the projectile aerodynamics at both the near-field and far field. A moving coordinate scheme for a multi-domain technique was employed to simulate the unsteady projectile flows with a moving boundary. The effect of a virtual mass was included to the unsteady, axisymmetric Euler equations. The present computations were validated with experimental results. It is noted that the computed results reasonably capture the major flow features such as shock waves, blast waves, vortical flows, etc, which are generated in launching a projectile up to supersonic speeds. The present computational method properly predicts the velocity, acceleration and the drag histories of the projectile.

2. Computational Analysis

2.1 Governing equations

With the recent development in computing capability and computational schemes as well, several kinds of moving boundary methods have been developed in computational fluid dynamics (CFD) area. Now the present level of the CFD is making highly complicated unsteady flows accurately predictable. In three spatial dimensions, the conservation equations are written in the following integral form:

$$\frac{d}{dt}\iiint Q dV + \iint \mathbf{F}\cdot\mathbf{n} dA = \iiint \mathbf{S} dV \tag{1}$$

where,

$$Q = \begin{pmatrix} \rho \\ \rho u_1 \\ \rho u_2 \\ \rho u_3 \\ E \end{pmatrix}, \qquad F_k = \begin{pmatrix} \rho u_k \\ \rho u_1 u_k + \delta_{1,kp} \\ \rho u_2 u_k + \delta_{2,kp} \\ \rho u_3 u_k + \delta_{3,kp} \\ E u_k + u_j \delta_{j,kp} \end{pmatrix} \tag{2}$$

$$\mathbf{u} = (u_1, u_2, u_3) \tag{3}$$

$$p = (\gamma - 1)\left(E - (1/2).u_m^2\right) \tag{4}$$

The source vector is added when the coordinate system fixed to a moving domain is used, as will be described later (see Sec. 2.2).

2.2 Moving coordinate method for multi-domain technique

The unsteady flows around the projectile discharged from a ballistic range and flying in the test section are numerically solved by using a multi-domain technique. In the present study, two coordinate systems and two domains are employed to simulate the projectile aerodynamics; the coordinate system A is fixed to the domain A about the flying object and the coordinate system B is fixed to the domain B near the launch tube of the ballistic range(see Fig.1). This means that two coordinate systems are moving away from each other with a flight speed of the projectile. By this reason, the present multi-domain technique slightly differs from that of Takakura et al. (1995) and Steger et al. (1983) in next two points.

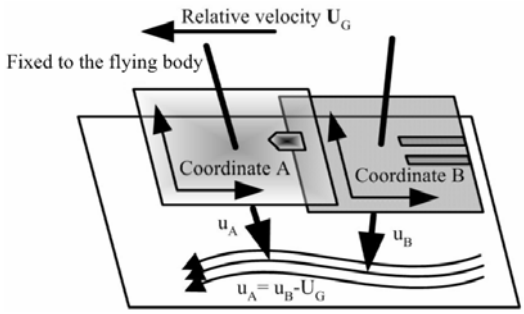

Fig. 1. Flow field observed from the moving coordinate.

Firstly, the governing equations must include the effect of virtual mass to simulate the projectile. Since the velocity of the moving grid, $U_g=(U_{g1}, U_{g2}, U_{g3})$, is uniform in the space within a domain, only the following source term should be included in Eq. (1) for each domain:

$$S = \begin{pmatrix} 0 \\ -\rho dU_{g1}/dt \\ -\rho dU_{g2}/dt \\ -\rho dU_{g3}/dt \\ -\rho\left(\mathbf{u} d\mathbf{U}_g/dt\right) \end{pmatrix} \tag{5}$$

Here assuming that the coordinate system A is moving with the relative velocity U_G to B, this speed is exactly identical to the flying speed of the projectile, which is determined by solving the Newton's equation of motion at every time step, with the initial speed given.

Second, in exchanging the physical values between domains, observable values on each coordinate system should be evaluated by the Galilean transformation. Let u_A and u_B be the fluid velocities observed in the coordinates A and B, respectively, then $u_A = u_B - U_G$ holds (see Fig. 1).

Therefore in the transformation from B to A, momentum M and total energy E are evaluated by

$$\mathbf{M_A} = \mathbf{M_B} - \rho U_G \tag{6}$$

$$E_A = E_B - \rho \mathbf{u_B}\cdot\mathbf{U_G} + (1/2)\rho \mathbf{U_G^2} \tag{7}$$

Similarly, in the transformation from A to B, the following holds:

$$\mathbf{M_B} = \mathbf{M_A} + \rho \mathbf{U_G} \tag{8}$$

$$E_B = E_A + \rho \mathbf{u_A}\cdot\mathbf{U_G} + (1/2)\rho \mathbf{U_G^2} \tag{9}$$

When we see the fluid motion from the coordinate system fixed to the moving object, the boundary condition on the moving wall becomes identical to that on the stationary wall, which is the advantage of the present computational method.

2.3 Numerical scheme

When Eq. (1) is applied on the structured-grid cell (ξ, η, ζ) with the symmetric condition in the ζ direction, we can obtain the following finite volume expression for axisymmetric flow:

$$\frac{d}{dt}\left(Q_{i,j}V_{i,j}\right) = \hat{F}^{\xi}_{i+1/2,j} - \hat{F}^{\xi}_{i-1/2,j} + \hat{F}^{\xi}_{i,j+1/2} - \hat{F}^{\eta}_{i,j-1/2} + \hat{D}F^{\xi}_{i,j} \quad (10)$$

$$\hat{F}^{\xi} = \mathbf{F}\cdot\mathbf{n}^{\xi}A^{\xi}, \quad \hat{F}^{\eta} = \mathbf{F}\cdot\mathbf{n}^{\eta}A^{\eta} \quad (11)$$

where A^{ξ} and A^{η} are the areas of cell surface, and n^{ξ} and n^{η} are the unit vectors normal to the cell surface, respectively. The difference of axisymmetric case from the two-dimensional case is that the pressure correction $\hat{D}F^{\varsigma}$ is added in symmetric form of conservation law equation (Vinokur, 1989).

The axisymmetric Euler equations with virtual mass are solved by the cell-centered finite volume method. The spatial discretization is executed by the third order Chakravarthy-Osher total variation diminishing (TVD) scheme (Chakravarthy & Osher, 1985), with MUSCL approach, improved in linearization (Takakura et al., 1987), and the time integration is carried out by the second-order Runge-Kutta scheme (Rizzi, 1982): when Eq. (11) is rewritten as

$$\frac{d}{dt}Q = \mathbf{f}(Q) \quad (12)$$

then,

$$Q^{(1)} = Q^{n} + \Delta t f\left(Q^{n}\right) \quad (13)$$

$$Q^{(2)} = Q^{n} + \frac{\Delta t}{2}\left[f\left(Q^{n}\right) + f\left(Q^{(1)}\right)\right] \quad (14)$$

$$Q^{(n+1)} = Q^{n} + \frac{\Delta t}{2}\left[f\left(Q^{n}\right) + f\left(Q^{(2)}\right)\right] \quad (15)$$

where, n denotes the value at time (n).

2.4 Computational and boundary conditions

The present moving coordinate method is applied to computation of flow phenomena when a projectile is discharged from the launch tube of a ballistic range. Figure 2 shows the computational domain and boundary conditions applied in the present study. The projectile is placed in the launch tube, where the initial conditions are maintained constant at pressure p_4, temperature T_4, and velocity u_4. The length of the launch tube is 200 mm and its diameter D_p is 20 mm. Still air outside the launch tube has the initial pressure p_1, temperature T_1, and velocity u_1. The computational domain extends up to a location of 267 mm away from the axis of the launch tube in transverse direction, but, in axial direction, it varies depending on the initial conditions applied in the present computations.

Free boundary conditions are applied to the left and upper boundaries of the present computational domain and the wall boundary conditions are applied to the wall of the launch tube and the right boundary of the present computational domain. The axisymmetric conditions are employed to reduce the computing effort of the full domain. At the right end of the launch tube, free boundary conditions are also applied to maintain the initial conditions (p_4, T_4, and u_4) during computation.

Figure 3 shows the computational grid system for the domains A and B overlapping at the initial state, where the base of the projectile is placed at a location inside the launch tube (see Fig. 2). In the present computation, the structured grid system is used. Several preliminary computations have been carried out to get the grid-independent solutions. The number of the computational grids was highly limited by the computing time and memory. The computational

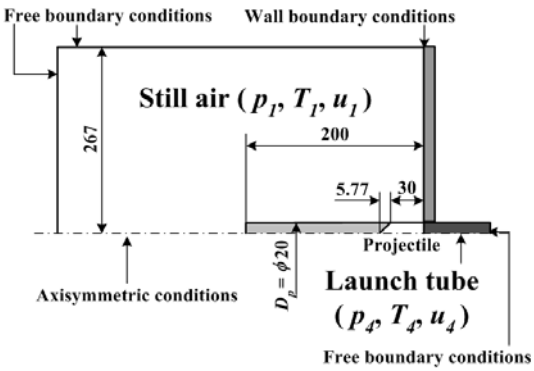

Fig. 2. Computational domain and boundary conditions.

grids for the moving domain and the fixed domain are about 800,000 and 700,000, respectively.

Figure 4 shows the three projectiles used in the present study. Cases 1 and 2 are of the same configuration as that of an axisymmetric body with a cone having a semi-apex angle of 30 degree, but with different projectile masses (M_p) to investigate the mass effects on the projectile aerodynamic characteristics. Meanwhile, Cases 1 and 3 have the same mass (M_p), but the projectile shapes are different. Case3 is the axisymmetric cylinder without the cone section. The projectile material is assumed to be aluminum.

Table 1 summarizes the computational flow conditions for the three cases mentioned above. Throughout all of the present computations, the still air outside the launch tube is kept at constant pressure p_1, temperature T_1 and velocity u_1 (0 m/s), while at the base of the projectile inside the launch tube, high-pressure and temperature states (p_4 and T_4) at t = 0, are maintained constant at 200MPa and 1000K, respectively. Such a state corresponds to the flow conditions obtained by firing an explosive inside the launch tube.

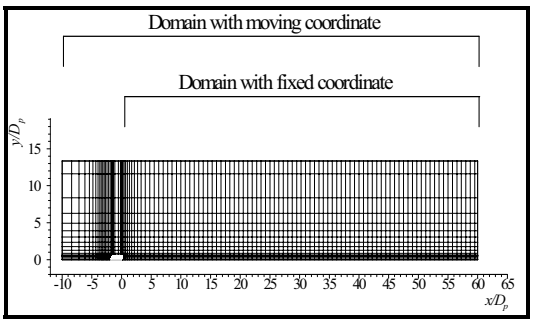

Fig. 3. Computational grid system.

3. Results and discussion

The present computations are validated using the flow visualization results of Schmidt & Shear (1975) in Fig. 5, where the upper half is the schlieren pictures and the lower half is the computed iso-density contours, and t is the time lapsed from the instant that the projectile starts to move inside the launch tube. The initial conditions behind the projectile are assumed to be p_4 = 1000 kPa, T_4 = 1000 K. It shows excellent agreement with the visualization pictures. The present computation predicts an identical flow field with that of Schmidt & Shear (1975), as the agreement between the basic flow features, such as the rate of blast wave development, starting vortex generation and the formation of the secondary shock wave in between the vortex pair, in both the cases is quite good.

Figure 6 shows the computed iso-pressure contours for Case 1. With the beginning of computations, the projectile moves from its initial position to the exit of the launch tube. At t=0.2096 ms, compression waves formed in front of the projectile due to the moving piston effect, are seen to be coalescing into a shock wave, while the projectile is moving still inside the launch tube. At t=0.3830 ms, the projectile is on the verge of discharging from the launch tube, and a jet flow is developed at the open end of the launch tube. A contact discontinuity is formed behind the shock wave which separates the still air outside the launch

Table 1. Computational conditions.

Model	p_1 (kPa)	T_1 (K)	u_1 (m/s)	P_4 (MPa)	T_4 (K)	u_4 (m/s)	M_p (kg)
Case 1	100	293	0	200	1000	0	0.0135
Case 2	100	293	0	200	1000	0	0.00675
Case 3	100	293	0	200	1000	0	0.0135

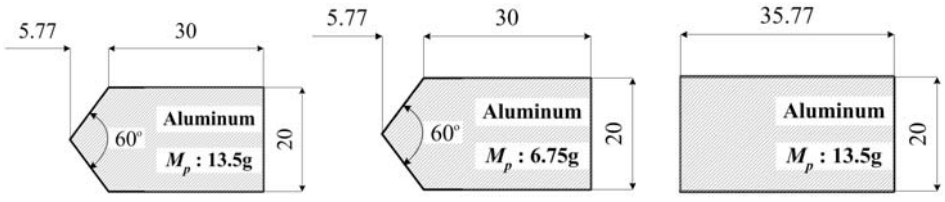

(a) Case 1 (b) Case 2 (c) Case 3

Fig. 4. Projectile configurations.

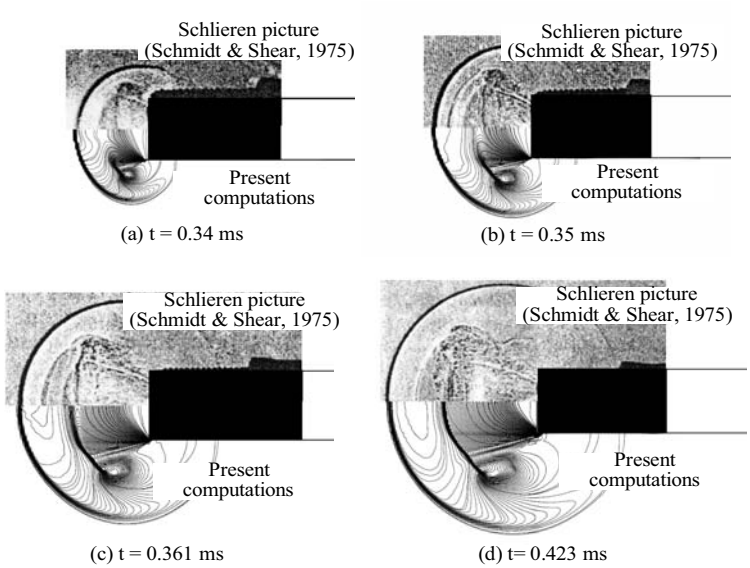

Fig. 5. Comparison of present CFD with the experimental results (Schmidt & Shear, 1975).

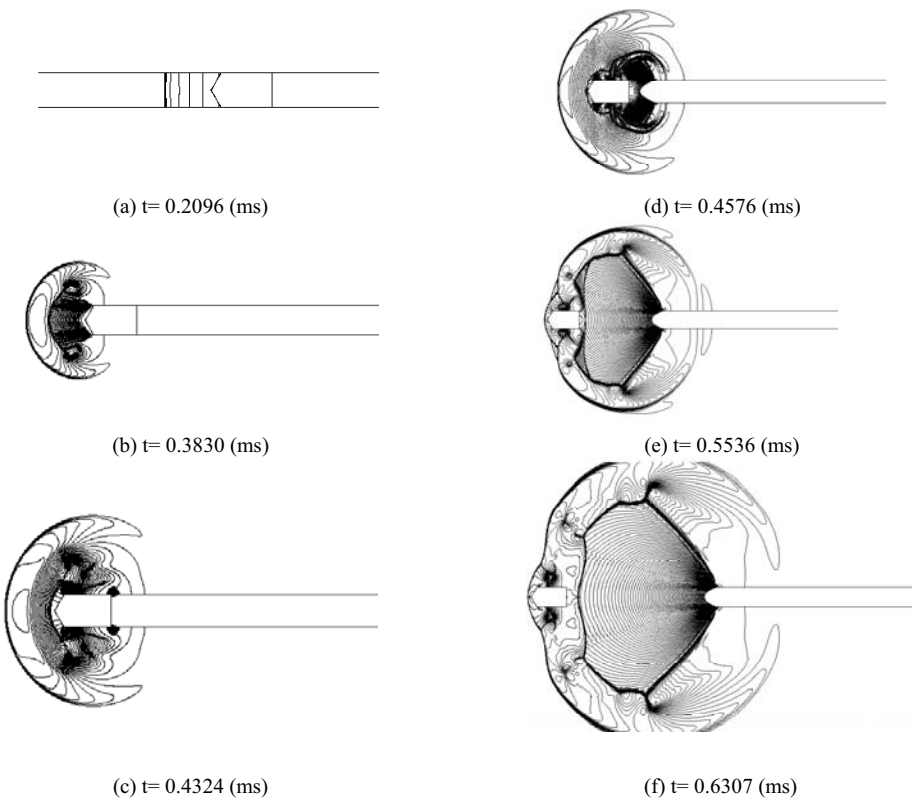

Fig. 6. Computed pressure contours around a flying projectile.

tube which has early been perturbed by the discharged shock wave and the gas in the under-expanded jet formed due to the discharge of the compressed air in front of the projectile. Strong vortices are also formed at both the edges of the contact discontinuity due to the impulsive start of the flow from the launch tube. All these flow features are associated with shock wave diffraction at the exit of the tube and constitute for the primary blast wave seen in such flow configurations (Kim & Setoguchi, 1999; Kim et al., 2002).

At t= 0.4324 and 0.4576ms, the projectile is shortly after discharging from the exit of the launch tube, and the first blast wave is spreading around. When the projectile is discharged from the launch tube, the high-pressure, high-temperature gas behind the projectile rushes out as a highly under expanded jet, forming the second blast wave consisting of a second contact discontinuity which separates supersonic jet ahead of the projectile and that behind the projectile. Unlike the first blast wave, the second blast wave develops in the radial direction as the axial component of the second blast wave is deteriorated due to its strong interaction with the supersonic jet ahead of the projectile and the shear layer. However, the wave system behind the second blast will be stronger as it moves into relatively slower background gas and the back ground flow becomes non-uniform too.

At t=0.5536ms, the projectile overtakes the contact discontinuity and the compression waves in the first blast wave where it encounters a very low speed gas. This leads to the formation of a detached bow shock wave in front of the projectile. It is also observed that a triple point is formed when the bow shock wave is interacting with the second blast wave. A second triple point is formed later when the projectile catches up the first blast wave at t=0.6307ms, while the first triple point is dissipated. At this point, the bow shock becomes stronger as it moves through still air. It is interesting to note that the projectile overtakes the blast wave completely within a very short distance from the exit of the launch tube.

The predicted velocity histories of the three different projectiles are presented in Fig. 7, where u_p is the projectile velocity, and C_1, C_2 and C_3 indicate the time instants at which the projectile is discharged from the launch tube, for Cases 1, 2 and 3, respectively. When the computations begin, the projectile accelerates suddenly inside the launch tube, and this instantaneous acceleration persists over a very short distance due to the inertia effect even after the projectile having discharged from the launch tube. This duration is strongly dependant on the projectile mass. Later, the projectile is decelerated due to aerodynamic drag effects.

It is clearly visible from Fig. 8 that how the projectile acceleration varies for each case. The impulsive acceleration of the projectile at the beginning of the computations suddenly decreases due to the wave drag from the compression waves in front of it. A sharp reduction in the acceleration can also be seen later when the projectile is discharged from the launch tube. From these plots, it is known that shape of projectile has a negligible effect on the velocity and the acceleration of the projectile in the near-field of the launch tube. However, the projectile velocity and acceleration are strongly affected by the mass of it. For a lighter projectile, the velocity will be more as seen from Fig. 7.

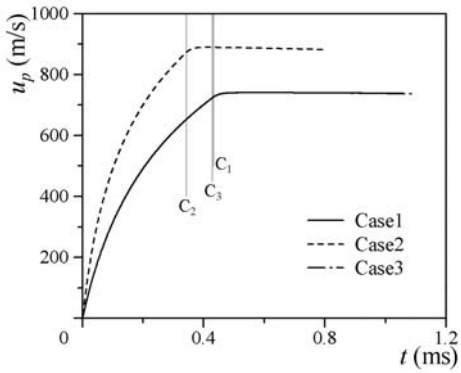

Fig. 7. Time histories of projectile velocity.

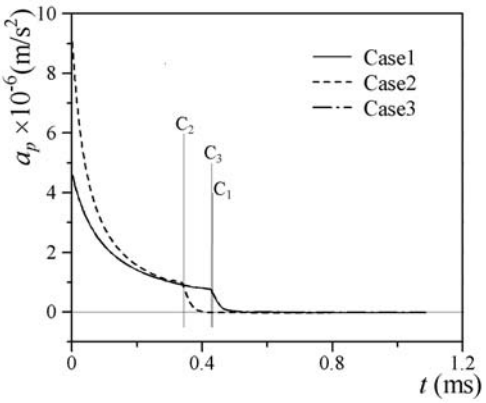

Fig. 8. Time histories of projectile acceleration.

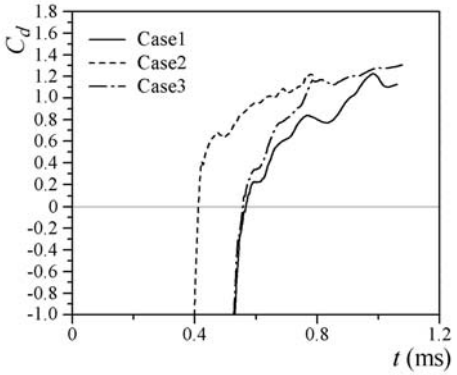

Fig. 9. Variation in drag coefficient with time.

Further, the drag coefficients of the projectiles can be computed to investigate the nature of unsteady drag forces acting on them. Here it should be noted that the present computations do not include any viscous and heat transfer effects. Therefore the entire drag force is composed of the pressure and wave drags due to the pressure difference between the front and rear sides of the projectile and the shock wave in front of it.

In the present study, the coefficient of aerodynamic drag C_d on the projectile is defined as,

$$C_d = \frac{2D}{\gamma p_1 M_a^2 A} \tag{16}$$

where, D is the drag force, A is the projected area of projectile, γ is the ratio of specific heats, p_1 is the pressure in front of projectile, and M_a is the Mach number of projectile.

Figure 9 shows the predicted C_d values of the three projectiles. The negative C_d values are due to the high-pressure at the base of the projectile inside the launch tube which makes the pressure drag negative or in other words, a thrust force. Upon discharging from the exit of the launch tube, the drag force on the projectile sharply increases, and it increases further with some fluctuations. These fluctuations in the drag coefficient are attributed to the unsteady aerodynamic loads acting on the projectile during the initial phases of flow transitions behind the blast waves. It is known from the C_d curves of Cases 1 and 3 that projectile shape affects the drag coefficient only after the projectile is discharged from the launch tube. This is expected as the unsteady flow patterns on the projectiles in these cases are entirely different owing to dissimilar projectile shapes when the projectile is outside the launch tube, while the flow characteristics do not differ much when the projectiles are inside the launch tube. On the other hand, irrespective of the projectile locations, the qualitative drag characteristics of Cases 1 and 2 do not differ significantly as they have the same configurations. However, the projectile in Case 2 being lighter, is discharged early, and is acted upon by a higher drag force due to higher acceleration.

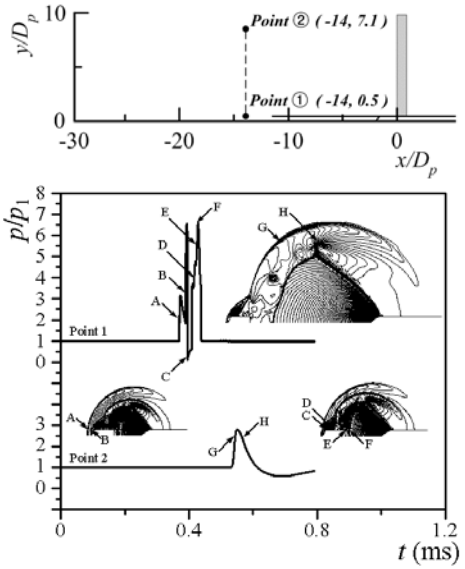

Fig. 10. Time histories of static pressures at the point ① and ② (Case 2).

In order to investigate the unsteady flow characteristics in the near-field of the launch tube in more detail, the static pressure variations at the points 1 and 2 for Case 2 are shown in Fig. 10. At point 1, the static pressure remains constant at p_1 before the blast wave reaches, and it suddenly increases due to the primary shock wave (denoted as A) of the first blast wave. The pressure rises sharply further when point 1 is swayed by the secondary shock wave (B) of the first blast wave. Then it decreases suddenly due to the expansion waves generated at the projectile shoulder, and increases further due to the shock waves (D and E) and the jump discontinuity (F) formed between the supersonic jet ahead of the projectile and that behind the projectile. Later, it drops to the p_1 level. It is noted that these strong pressure fluctuations significantly influence the flight stability of the projectile as seen from the drag coefficient curves. The inherent unsteadiness of this flow field accounts for the difference between the steady and

unsteady drag characteristics of the flying projectiles. At point 2, the static pressure distribution appears to be a typical N-wave, so called "sonic boom." The shoot up and the sharp drop in the static pressure are due to the shock wave (G) and the expansion waves (H), respectively.

In order to look into the projectile configuration effects on the pressure fluctuations, the static pressure variations at points 1 and 2 for Case 3 are shown in Fig. 11. It should be noted that the blast waves of the projectiles reach the point 1 at different timings. On account of the reduced acceleration and velocity due to the heavier projectile, the amplitudes of the static pressure fluctuations (A, B and C) generated by the first blast wave at point 1 are smaller than those in Fig. 10. However, the pressure fluctuations due to the second blast wave (E) are larger in amplitude. As explained early, here, the secondary blast wave is spreading in the radial direction to a much slower gas than that in Case 2, consequently leading to a stronger wave system compared to that in Case 2. At point 2, the quantitative pressure variation seems not to be much different from that in Fig. 10 as the velocities of both the projectiles differ by a great amount. However, the pressure fluctuations qualitatively disagree in terms of the sharpness in the pressure rise and drop. If both had comparable velocities so that their blast waves reached point 2 at the same time, the sonic boom in Case 3 would be much different from that in Case 2 both qualitatively and quantitatively. Thus, it can be appreciated that the projectile configuration has an important influence on the pressure fluctuations in the near-field.

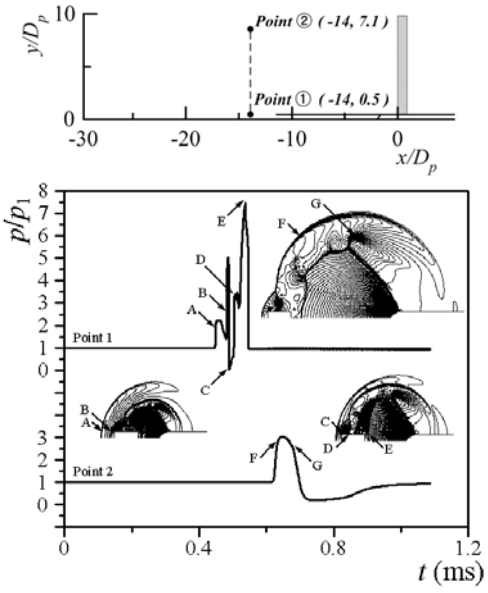

Fig. 11. Time histories of static pressures at the point ① and ② (Case 3).

4. Conclusions

A computational fluid dynamics method using a moving coordinate technique has been applied to simulate the near-field aerodynamics of the projectile which is launched from a ballistic range. The effect of virtual mass was added in the unsteady, axisymmetric Euler equation systems which were numerically solved using the third order Chakravarthy-Osher total variation diminishing scheme, with MUSCL approach. The projectile mass and configuration were changed to investigate the effect on the unsteady flow structures in the near-field. The present computations were validated with some other available experimental results. It is known that the computed results reasonably capture the major flow features, such as shock waves, blast waves, vortical flows, etc. which are generated in launching a projectile up to a supersonic speed. The present computational method properly predicts the velocity, acceleration and drag histories of the projectile.

The unsteady aerodynamic characteristics of the projectile are significantly different from the steady characteristics. The fluctuations of the drag coefficient in the near-field of the launch tube reveal the effects of the unsteady flow structures. It is also observed that the projectile mass and its configuration are the major factors which determine the flow patterns and hence the unsteady aerodynamic loads on the projectile during its flight in the near-field.

Nomenclature

A : Area, m^2
D : Drag force, N
E : Total energy, J
F : Convection flux tensor
M : Momentum, $kg.m/s^2$
M_a: Mach number
n : Outer unit normal vector at the cell surface
p : Pressure N/m^2
Q : Conservative variable Vector
S : Source Vector
T : Temperature, K
T : Time, s

U	: Velocity vector
u	: Velocity in X-direction, m/s
v	: Velocity in Y-direction, m/s
x, y, and z	: coordinate axes

Greek letters

γ	: Ratio of specific heats
ρ	: Density, kg/m^3
ξ, η and ζ	: Transformed coordinates

Sub-scripts:

G, g	: Grid
1, 2 and 3	: Coordinate directions

References

Baker, W. B., 1974, "Explosion in Air," University of Texas Press, Austin.

Chakravarthy, S. R. and Osher, S., 1985, "A New Class of High Accuracy TVD Schemes for Hyperbolic Conservation Laws," *AIAA paper 85-0363*.

Erdos, J. I. and Del Guidice, P. D., 1975, "Calculation of Muzzle Blast Flow Fields," *AIAA J*., Vol. 13, p. 1048.

Glass, I. I., 1974, "Shock Waves and Man," The University of Toronto Press, Canada.

Jiang, Z., Takayama, K. and Skews, B. W., 1998, "Numerical study on Blast Flow Fields Induced by Supersonic projectiles Discharged from Shock Tubes," *Physics of Fluids*, Vol. 10(1), p. 277.

Kim, H. D. and Setoguchi, T., 1999, "Study of the Discharge of Weak Shocks from an Open End of a Duct," *Journal of Sound and Vibration*, Vol. 226, p. 1011.

Kim, H. D., Lee, D. H. and Setoguchi, T., 2002, "Study of the Impulse Wave Discharged from the Exit of a Right-angle Pipe Bend," *Journal of Sound and Vibration*, Vol. 259, p. 1147.

Merlen, A. and Dyment, A., 1991, "Similarity and Asymptotic Analysis for Gun Firing Aerodynamics," *J. Fluid Mechanics*, Vol. 225, p. 497.

Pope, A. and Goin, K. L., 1963, "High-Speed Wind Tunnel Testing", *John Wiley and Sons*, New York.

Rizzi, A., 1982, "Damped Euler-Equation Method to Compute Transonic Flow around Wing-Body Combinations," *AIAA J*., Vol. 20(10), p. 1321.

Schmidt, E. and Shear, D., 1975, "Optical Measurements of Muzzle Blasts," *AIAA, J*., Vol. 13, p. 1086.

Steger, J. L., Dougherty, F. C. and Benek, J. A., 1983, "A Chimera Grid Scheme," *Advances in Grid Generation ASME FED-5*, p. 59.

Sun, M., Siato, T., Takayama, K. and Tanno H., 2005, "Unsteady Drag on a Sphere by Shock Loading," *Shock Waves*, Vol. 14, p. 3.

Takakura, Y. and Higashino, F., 1997, "Numerical Study on the Sonic Boom Simulator Using a Ballistic Range," *21st International Symposium on Shock Waves (ISSW21)*, Great Keppel Island, Australia, July 20-25.

Takakura, Y., Higashino, F. and Ogawa, S., 1997, "Unsteady Flow Computations on a Flying Projectile within a Ballistic Range," *Computers & Fluids*, Vol. 27(5-6), p. 645.

Takakura, Y., Ishiguro, T. and Ogawa, S., 1987, "On the Recent Difference Schemes for the Three-Dimensional Euler Equations," *AIAA paper 87-1151.*

Takakura, Y., Ogawa, S. and Wada, Y., 1995, "Computations of A Transonic Wind-Tunnel Flows about a Fully Configured Model of Aircraft by Using Multi-Domain Technique," *AIAA Paper 93-3022.*

Vinokur, M., 1989, "An Analysis of Finite-Difference Formulations of Conservation Laws," *J. Computational Physics*, Vol. 81, p. 1.